Scripta Materialia 158 (2019) 110–115

Contents lists available at ScienceDirect

Scripta Materialia

journal homepage: www.elsevier.com/locate/scriptamat

High-temperature damage-tolerance of coextruded, bioinspired ("nacre-like"), alumina/nickel compliant-phase ceramics

Ryan P. Wilkerson [a,b], Bernd Gludovatz [c], Jon Ell [a,b], Jeremy Watts [d], Gregory E. Hilmas [d], Robert O. Ritchie [a,b,]*

[a] Department of Materials Science & Engineering, University of California, Berkeley, CA 94720, USA
[b] Materials Sciences Division, Lawrence Berkeley National Laboratory, Berkeley, CA 94720, USA
[c] School of Mechanical and Manufacturing Engineering, UNSW Sydney, NSW 2052, Australia
[d] Department of Materials Science & Engineering, Missouri University of Science and Technology, Rolla, MO 65409, USA

ARTICLE INFO

Article history:
Received 6 August 2018
Received in revised form 25 August 2018
Accepted 26 August 2018
Available online xxxx

Keywords:
Extrusion
Nacre
Biomimetic ceramics
High temperature
Crack-growth resistance

ABSTRACT

In this study, we use the coextrusion process to make high volume-fraction, nacre-like brick-and-mortar alumina structures with <10% nickel between the ceramic bricks. We perform strength and toughness tests on these compliant-phase aluminas at temperatures up to 900 °C, both to explore the evolution of toughening with changes in the mortar plasticity and to evaluate the viability of these materials at elevated temperatures. We find that temperature plays an important role in the mechanical performance of these materials. Specifically, we observe that crack-growth resistance can be improved at higher temperatures due to enhanced ductility in the metallic mortar.

In the search for the next-generation lightweight structural materials, ceramics are of interest for industrial applications involving extreme environments and elevated temperatures, owing to their high specific strength, creep resistance and elastic stiffness, as well as low thermal expansion and good corrosion resistance. However, their strong atomic bonding and high Peierls-Nabarro stress act to confer brittleness, resulting in severely compromised ductility and toughness. While advances have been made to improve their toughness, the development of ceramics with significant crack-growth resistance is still limited. Nature, however, is adept at creating lightweight damage-tolerant materials using brittle minerals and soft biopolymers with relatively meagre mechanical properties [1–3]. Nacre ("Mother-of-Pearl" in abalone shells) provides a notable example of a ceramic (~95 vol% aragonite) with exceptional strength, toughness and wear resistance, despite having the composition of chalk [4–9].

Nature's design invariably involves hierarchical structures [1,2] with ingenious gradients [10]. Indeed, nacre displays energetic toughness values that are over two orders of magnitude higher than its constituent materials through the formation of a "brick-and-mortar" microstructure, where aragonite "bricks" are bonded together with a protein biopolymeric "mortar" [4–9]. Here, strength derives from the hard-ceramic bricks, while the mortar induces ductility through limited brick sliding; combined, these properties generate crack-growth resistance through multiple toughening mechanisms, principally crack deflection and brick pull-out leading to crack bridging [9].

Nacre's brick-and-mortar structure has been the subject of significant modeling [8,9,11–15], which has confirmed that high aspect-ratio, micrometer-sized bricks with <10 vol% of a ductile mortar phase can provide optimal mechanical performance [11,12]. Although most synthetic nacre-like ceramics have been processed with polymeric mortars, modeling suggests that the higher shear/tensile resistance of a metallic mortar can further enhance the strength and toughness of these materials, provided the mortar strength does not exceed that of the ceramic bricks (whereupon the bricks fracture and damage-tolerance is lost) [11].

There have been numerous studies to develop synthetic nacre. Of the "top-down" approaches, freeze-casting has shown most promise as a highly-tunable, bulk-processing, method which produces layered ceramic lamellae through the directional freezing of aqueously-dispersed powder that eventually becomes the bricks, while the mortar phase is infiltrated afterwards [16–23]. However, while the mechanical properties of freeze-cast structures have been good, achieving >80 vol%

* Corresponding author at: Materials Sciences Division, Lawrence Berkeley National Laboratory, Berkeley, CA 94720, USA.
E-mail address: roritchie@lbl.gov (R.O. Ritchie).

https://doi.org/10.1016/j.scriptamat.2018.08.046
1359-6462/

of ceramic has been exceedingly difficult, particularly when infiltrating metallic mortars because they generally cannot wet ceramics. "Bottom-up" processing has also been used where the mortar is included throughout the consolidation [24–29]. Many such techniques use platelet phases and functionalized mortar surfaces, with self-assembly methods such as sedimentation, slip casting and tape casting, but sample volumes made by such techniques are small; moreover, there have been few attempts to incorporate metallic mortars [19,29]. One exception has been processing using coextrusion, which appears to be a viable alternative method for processing nacre mimetic structures with high ceramic volume-fractions exceeding ~90 vol% [30,31].

Coextrusion permits the manipulation of ceramic powders in a thermoplastic suspension to produce a core/shell architecture that can be formed into a brick-and-mortar structure. Our previous studies [30,31] on this processing method have shown that brick-and-mortar structures containing a low (<10 vol%) metallic mortar content can be made, which display many of the extrinsic toughening mechanisms (induced by crack-tip shielding [32]) seen in nacre. The brick size achievable with coextrusion is still much coarser than natural nacre, and fracture occurs along the mortar/brick interface instead of within the mortar itself. This means that although the structure can still induce inter-brick displacements to confer toughness, the beneficial effect of the higher strength of metallic mortars [11] is not exploited; moreover, failure at weak mortar/brick interfaces can cause low material strength. Accordingly, the full potential of nacre-like toughening in bioinspired ceramic brick-and-mortar structures has still yet to be realized.

Here we examine the effects of elevated temperatures on the mechanical properties of coextruded, nacre-like, alumina nickel compliant-phase ceramics from ambient temperature to 900 °C in air. We find that the fracture-toughness behavior of these brick-and-mortar aluminas progressively improves up to 800 °C, in part because at high temperature, inter-brick failure occurs within the metallic interphase rather than along the nickel/ceramic interfaces. Interfacial failure at lower temperatures results from the strength of the nickel mortar being higher than the interfacial strength, whereas for optimal properties, this interfacial strength should exceed the mortar strength but remain below the fracture strength of the ceramic. Increasingly higher temperatures provide an effective means to tailor these properties, specifically to reduce the mortar strength [33,34] so that it can plastically deform before interfacial failure. Therefore, a rationale for this study is to discern whether these alumina compliant-phase ceramics containing a metallic Ni mortar can be tuned to operate at high temperatures with optimal mechanical properties by confining the vital inter-brick displacements to be within the mortar phase. As such, it would represent the first study to observe ductile failure in a nacre-like high volume-fraction ceramic within the metallic compliant phase.

Alumina nickel brick-and-mortar ceramics were produced using a coextrusion assembly (Fig. 1A) in conjunction with hot-drawing to produce 200-μm Al_2O_3/NiO core/shell filaments which were subsequently laminated into oriented sheets using the process described in ref. [31]. These oriented sheets were then layered, offsetting each layer by 45°, to produce the microstructure shown in Fig. 1B. Following the build-up of oriented sheets into a brick-and-mortar structure, the thermoplastic binder was burnt-off to leave a ceramic green body that was heated in argon to 1400 °C, hot-pressed at 32 MPa for 30 min, before cooling to 25 °C. The NiO reduced to Ni during hot pressing leaving a final microstructure of alumina bricks bound with 10.2 vol% metallic nickel mortar.

The microstructure was characterized with scanning electron microscopy (SEM), using secondary and backscatter electron imaging at 20 keV, by a well-formed brick-and-mortar architecture normal to the hot-pressing direction (Fig. 1B); the ceramic "bricks" were ~185-μm wide and ~75-μm thick, joined by ~6.9-μm thick nickel mortar with an interconnectivity, measured using a contiguity-based approach [30,31], of ~89%.

To evaluate mechanical properties, flexural strength and crack-growth resistance-curve (R-curve) toughness tests were performed

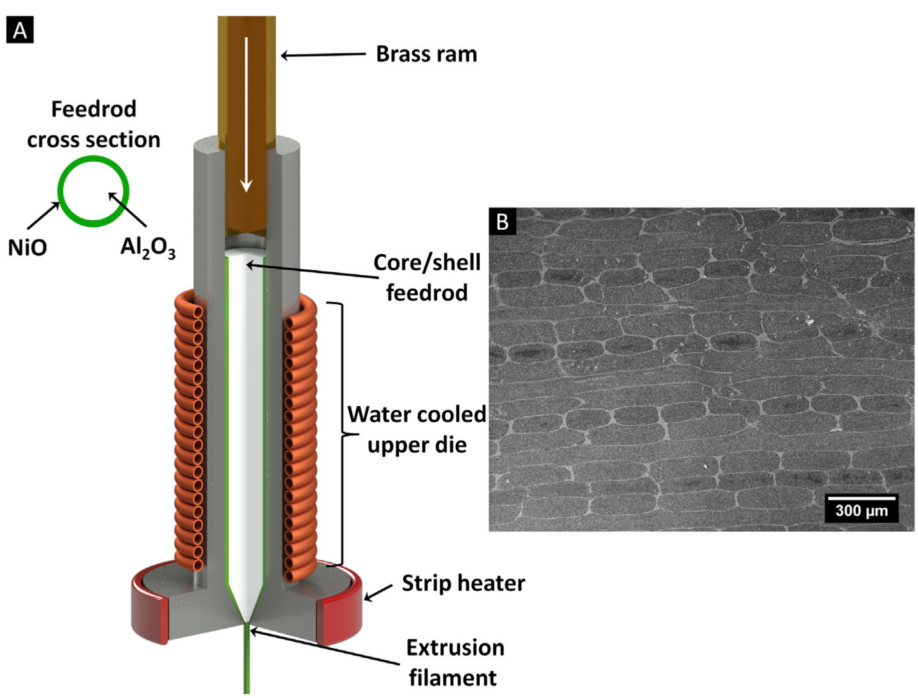

Fig. 1. (**A**) Schematic of the coextrusion assembly consisting of a water-cooled feedrod chamber with a reducing cone which is heated to improve the plasticity of the thermoplastic binder. The core to shell ratio is maintained through the extrusion process, producing a filament of the specified diameter determined by the outlet diameter. (**B**) Scanning electron micrograph of the resulting Al_2O_3/10Ni brick-and-mortar structure. The nickel mortar is highly continuous, and the brick size has been minimized through the hot drawing of filament from the extruder head to produce an optimal compliant-phase ceramic.

in air on the Al_2O_3/10Ni ceramic between ambient temperature and 900 °C. For strength tests, flexural beams were machined from identical billets to the B-type specification (3 × 4 × 45 mm), in accordance with ASTM Standard C1211-18 [35], and polished to a 1-μm diamond finish with chamfered long edges. These specimens tested in four-point bending (four tests at each temperature) in an open-air furnace on an Instron 5881 electro-mechanical testing machine (Instron Corp., Norwood MA) at a crosshead speed of 0.1 mm/min at 25°, 600°, 700°, 800° and 900 °C. A high-temperature linear-variable-differential transformer (LVDT), in contact with the tensile surface, was used to measure displacement.

Elevated temperature R-curve tests were performed at the same five temperatures in the same open-air furnace and testing machine in three-point bending at a displacement rate of 0.05 mm/min, using four single-edge-notched bend SE(B) bars at each temperature. The SE(B) bars (4 × 4 mm) were first polished and micro-notched (using a razor blade immersed in 2-μm diamond paste) to a ~15 μm notch-root radius at a crack length of half the width. Samples were loaded until cracking commenced, denoted by small (~2%) load drops, and then partially unloaded periodically to assess crack extension, Δa, from specimen-compliance measurements using the LVDT in contact with the bottom of the bar.

The fracture toughness was evaluated using nonlinear-elastic fracture-mechanics using the J-integral, in general accordance with ASTM Standard E1820 [36]. Specifically, J_R crack-resistance curves under plane-strain conditions were determined from the sum of the elastic contribution, K_{Ic}^2/E', where K_{Ic} is the linear-elastic fracture-toughness and $E' = E/(1-\nu^2)$ (E is Young's modulus, ν is Poisson's ratio), and nonlinear-elastic contribution, $1.9A_{tot}/Bb$, where A_{tot} is area under the load vs. load-line displacement curve, B is the specimen thickness, and b is the uncracked ligament length. ASTM Standard E1820 specifies that for strictly valid results, the maximum crack extension is $\Delta a_{\max} = 0.25b_0$, where b_0 is the initial uncracked ligament length.

To quote toughness in terms of the stress-intensity, K, the mode-I J-K equivalence, $K_J = (J\,E')^{1/2}$, was used to convert J_{Ic} to K_{JIc}. Valid J-dominance was maintained as the size-requirement of $b > 10\,J/\sigma_{flow}$ (σ_{flow} was equated to the flexural strength) was met for all R-curves. No data were collected where the R-curves took a "concave-up" appearance; this is an indication of large-scale bridging where toughness values become distinctly size- and geometry-dependent [17].

The elastic modulus E was determined using impulse excitation and calculated with a modified long-bar approximation using ASTM Standard C1259-15 [37]. Poisson's ratio for alumina was taken as $\nu \sim 0.23$.

The flexural strength of the Al_2O_3/10Ni microstructure as a function of temperature is shown in Fig. 2A. Tests revealed that after crack initiation, stable cracking ensued with no evidence of catastrophic fracture. The strength levels remain essentially constant between 25° and 800°C. Specifically, we see a marginal increase (~11%) between 25°C (158 ± 24 MPa) and 700 °C (175 ± 15 MPa), probably due to relaxation of residual stresses on cooling from 1400 °C resulting from the thermal-

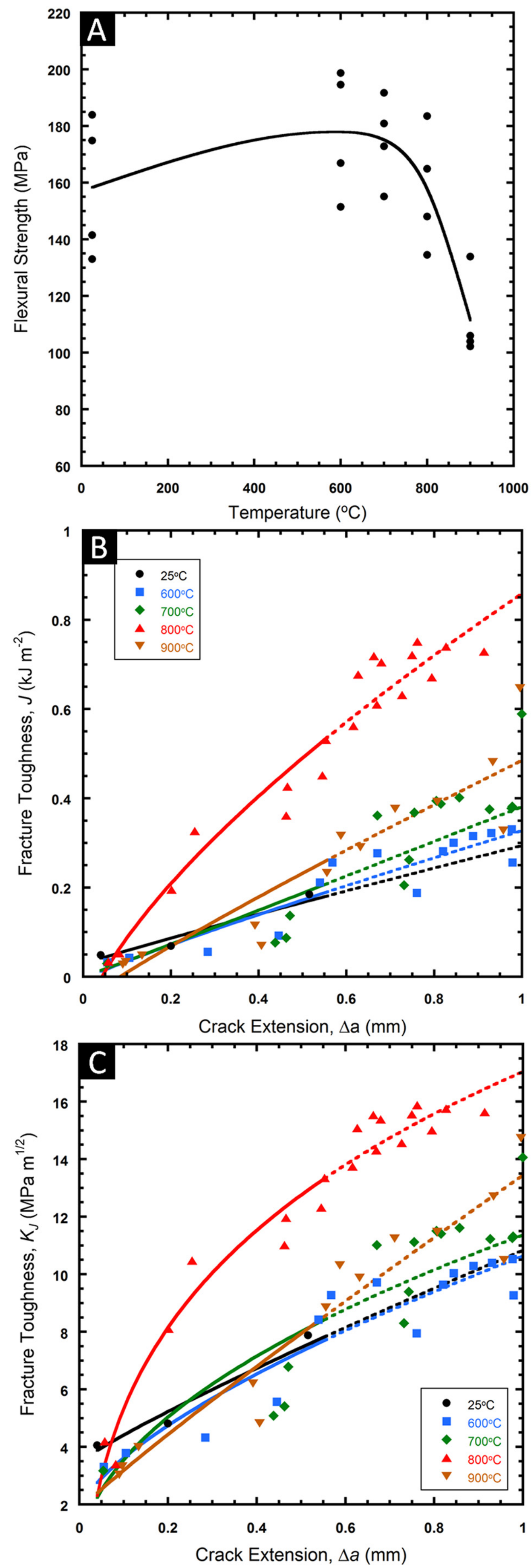

Fig. 2. Mechanical properties of the Al_2O_3/10Ni ceramic as a function of temperature (25° to 900 °C). (**A**) Flexural strength, measured in four-point bend tests, shows a marginal increase (~17 MPa) from 25° to 600 °C, possibly due to a reduction in residual stresses, with a decrease at 700 °C and a marked drop above 800 °C. Fracture toughness R-curves based on (**B**) J-integral measurements and (**C**) back-calculated K values, generated using a multi-specimen approach involving a minimum of four separate experiments. Essentially identical R-curves are seen between 25° and 600 °C, with a small increase at 700 °C, followed by a marked increase at 800 °C where inter-(ceramic) brick displacements involve ductile tearing within the mortar phase occurs instead of interfacial mortar/brick failure. The toughness decreases at 900 °C, associated with a significant loss in strength. Solid lines represent data that is considered strictly valid ($\Delta a_{\max} = 0.25b_0$), according to ASTM Standard E1820 [36], while dashed lines indicate when Δa has exceeded this conservative maximum crack-extension limit.

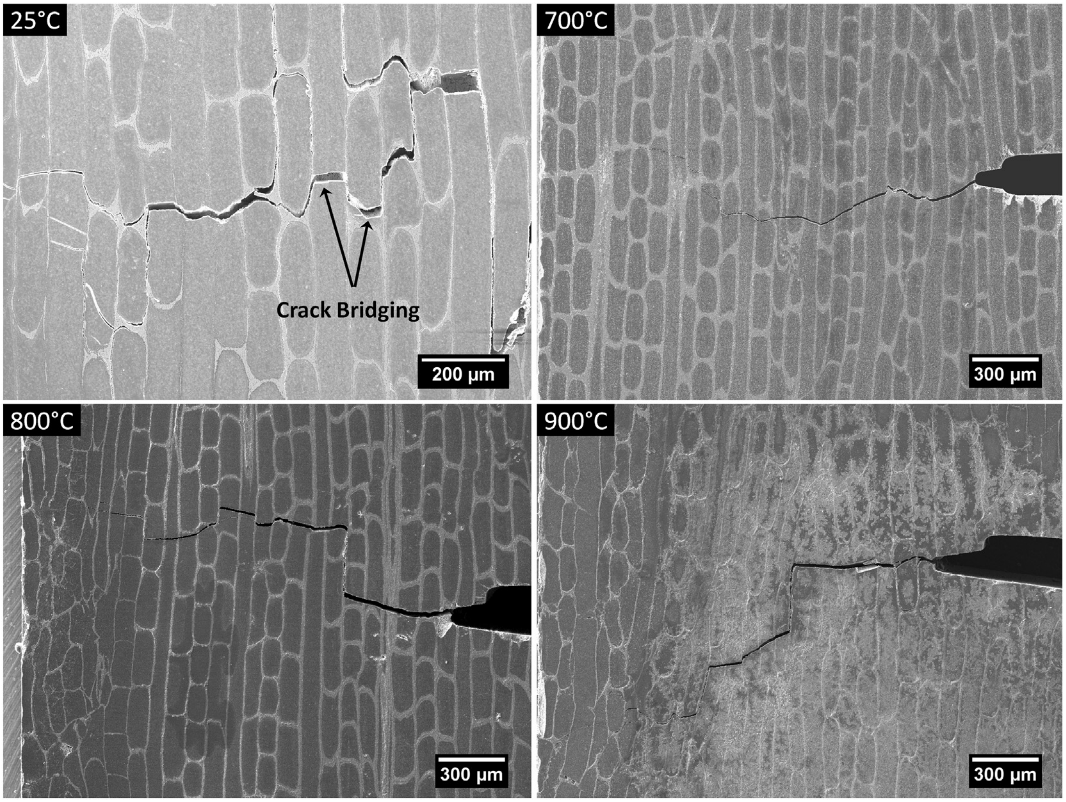

Fig. 3. Mechanistic aspects of rising R-curve toughness behavior in the Al_2O_3/10Ni ceramic. SEM micrographs of the crack paths from R-curve specimens seen at each temperature. Fracture trajectories between 25° and 700 °C were virtually identical, with the crack either fracturing bricks or propagating along the brick-mortar interfaces. Although such interfacial inter-brick displacements are not optimal, they can still result in brick pull-out and resultant crack bridging, At 800° and 900 °C, considerably more crack deflection is apparent, with cracking following a path within the nickel mortar (Fig. 4); this corresponds to the larger increase in R-curve behavior at 800 °C, although softening (Fig. 2A) and oxidation of the Ni mortar to NiO at higher temperatures, shown by the white scale in the vicinity of the notch, causes the toughness to drop at 900 °C.

expansion mismatch between Ni and Al_2O_3,[1] and a marginal decrease (~10%) at 800 °C (158 ± 21 MPa). At 900°C, however, a ~30% decrease (111 ± 15 MPa) occurs. As pure alumina does not display much reduction in strength between 25° and 900 °C [31], any strength changes for the Al_2O_3/10Ni ceramic is ascribed to softening of the interphase Ni (nickel's yield strength at 900 °C is some 75% lower than its room-temperature strength [34]). These results indicate that this material's maximum operable temperature is ~800 °C before properties start to deteriorate.

Based on fracture-toughness tests between ambient and 900 °C for the Al_2O_3/10Ni ceramic, the J-based and back-calculated K_J-based R-curves are presented in Fig. 2B,C, and notably show that this nacre-like structure does not fracture catastrophically but rather sustains stable cracking for extensions of ~1 mm or more. In terms of crack-initiation (4 ± 0.5 $MPa{\cdot}m^{1/2}$) and crack-growth toughness values, there is little to no change in properties between 25° and 600 °C, with a maximum ASTM "valid" toughness value of 8 $MPa{\cdot}m^{1/2}$. At 700 °C, the R-curve rises to 9 $MPa{\cdot}m^{1/2}$ and even further at 800 °C to ~13 $MPa{\cdot}m^{1/2}$, after which it drops to ~9 $MPa{\cdot}m^{1/2}$ at 900 °C. It should be noted that although these values are strictly valid in terms of the maximum crack extension allowed by ASTM Standard E1820 for our specimen sizes ($\Delta a_{\max} = 0.25b_0 = 550$ μm), the R-curve data continue to trend upwards beyond that, notably with the Al_2O_3/10Ni ceramic displaying a maximum toughness of 10 $MPa{\cdot}m^{1/2}$ between 25° and 700 °C, as high as 16 $MPa{\cdot}m^{1/2}$ at 800 °C, before falling to 13 $MPa{\cdot}m^{1/2}$ at 900 °C.[2]

Images of the corresponding crack trajectories are largely consistent with these results (Fig. 3). Samples fractured at 600° and 700 °C displayed similar crack paths that were essentially identical to those at 25 °C, with the cracks fracturing bricks or propagating along the brick-mortar interfaces. The observation that the cracks pass through the brick phase with inter-brick displacements and subsequent cracking occurring not within the metallic mortar phase but along the Al_2O_3/Ni interface at 700 °C and below is not ideal for properties; as noted above, the interface failure does provide the inter-brick sliding essential for toughness in these structures – brick pull-out and resultant crack bridging by interlocking bricks is evident – but the optimal effect for strength and toughness from the higher shear/tensile resistance of the metallic mortar is short-circuited, as the mortar provides little effect outside of offering a weak interface to direct the crack path. To date, this problem has plagued most brick-and-mortar ceramic structures containing a metallic mortar, as the ceramic-brick/metallic mortar interfaces are simply too weak. This not only limits toughening by crack bridging, but further acts to severely compromise the strength. However, this issue appears to be alleviated in the present structures at higher temperatures, where the strength of the nickel mortar is lower. At 800 °C, considerably more crack deflection is apparent, with further evidence

[1] Similar effects are seen in nuclear graphite, which becomes stronger and tougher with increasing temperature up to 1000°C from relaxation of processing-induced residual tensile stresses [38].

[2] R-curve at 25 °C is ~30% lower than those in previous studies [31] on earlier batches of material. This may be associated with small differences in the processing or in the different compliance-based method to measure crack extensions; due to possible microcracking on unloading, the current results may be more conservative in the form of slightly shallower R-curves.

of brick pull-out and consequent crack bridging; however, most importantly, the cracking now follows a path *within* the nickel mortar and not along the interface, which was confirmed using x-ray diffraction of matching fracture surfaces in the SEM to see nickel on both sides of the interfacial crack (this was not the case at lower temperatures). The fact that the inter-brick sliding is now accommodated within the mortar, with the associated plastic deformation and ductile damage of the metallic phase (Fig. 4), i.e., the interface strength exceeds the mortar strength, is responsible for the large increase in R-curve toughness at 800 °C. Indeed, the measured toughness at this temperature rises to ~16 MPa·m$^{1/2}$, which is almost an order of magnitude tougher than nanocrystalline alumina [39] and roughly twice that of alumina, grain-oriented to promote grain bridging [40]. However, the strength of our nacre-like ceramic is still not optimum due to the coarse nature of the coextruded structure.

At 900 °C, there is a significant degradation in strength and toughness, as this is clearly too high a temperature for the nickel to operate [34]. Indeed, this is consistent with observations of significant oxide scale, consisting primarily of NiO, on the 900 °C specimens (seen near the crack in Fig. 3).

However, R-curve behavior was observed at all temperatures between ambient and 900 °C, which results from the prime function of nacre-like structures, to induce stable cracking and avoid sudden catastrophic fracture. With increasingly steep R-curves and toughness values rising from ~10 to 16 MPa·m$^{1/2}$ between 25° and 800 °C, the current materials are among the toughest alumina ceramics on record. This is unusual as most ceramics, including alumina [33], generally display lower toughness at increasing temperature. Here, however, a major contribution to the higher elevated-temperature toughness results from the inter-(ceramic) brick displacements being localized within

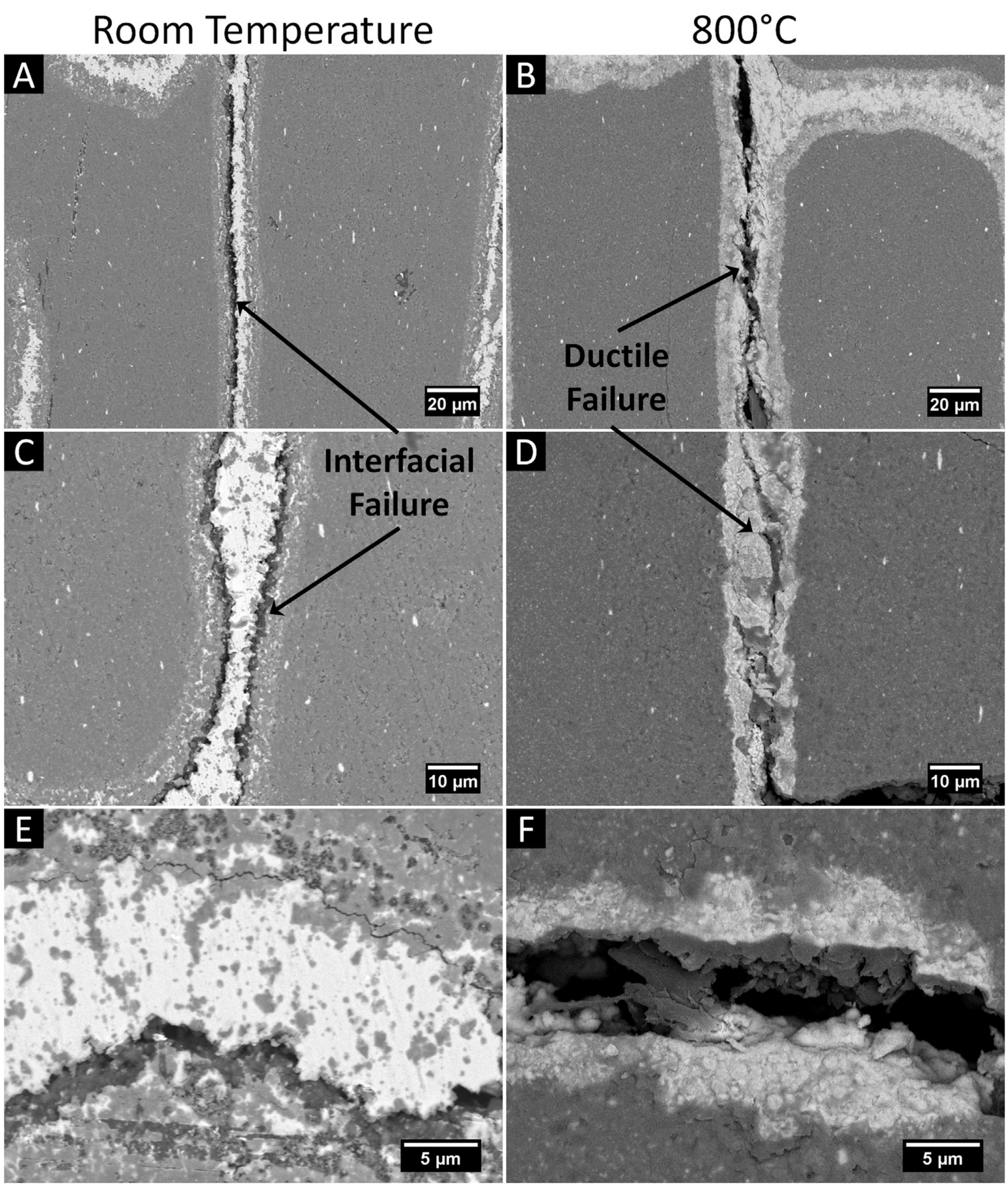

Fig. 4. SEM images taken in the backscatter electron (BSE) imaging mode to enhance the contrast between the Al_2O_3 bricks and Ni mortar of the coextruded Al_2O_3/10Ni ceramic samples fractured at room temperature (**A**,**C**,**E**) and 800 °C (**B**,**D**,**F**) at matching magnifications. It can be clearly seen how the fracture mode changes between ambient and high temperature, with cracking being contained within the mortar at high temperatures, and interfacial failure along the Al_2O_3/Ni interface at room temperature. In particular, **D** and **F** show ductile tearing within the metallic mortar phase, behavior that is unique to high-temperature failure in this material.

the nickel mortar leading to ductile failure of the metallic phase, rather than involving the ceramic-metal interface failure observed at lower temperatures. Moreover, unlike the similar nacre-like alumina structures containing a polymeric mortar, the current brick-and-mortar aluminas with a Ni mortar clearly become more viable for structural applications with increasing temperature up to 800 °C.

We conclude that:

1. Coextrusion is a viable method of making nacre-like brick-and-mortar microstructures consisting of ceramic bricks and low quantities of a metallic mortar.
2. Our ~90-vol% alumina containing a nickel mortar showed flexural strengths of 150–200 MPa between 25° and 800 °C, with fracture-toughness values rising to ~16 $MPa \cdot m^{1/2}$ at 800 °C.
3. Rising R-curves were observed at all temperatures with evidence of stable cracking, resulting from crack deflection, brick pull-out and crack bridging in the brick-and-mortar structure.
4. Whereas inter-brick displacements are critical to prevent a loss in damage-tolerance, the superior toughness at 800°C results from these displacements being contained within the metallic mortar, rather than involving metal/ceramic interface failure.

Data availability

The data that support the findings of this study are available from Dr. Wilkerson (email: rwilkerson@berkeley.edu) upon reasonable request.

Acknowledgements

This work was supported by the Mechanical Behavior of Materials Program (KC-13) at the Lawrence Berkeley National Laboratory, funded by the U.S. Department of Energy, Office of Science, Office of Basic Energy Sciences, Materials Sciences and Engineering Division, under contract no. DE-AC02-05CH11231. The authors would also like to thank their collaborators at Missouri University of Science and Technology, Rolla for the use of their facilities.

References

[1] U.G.K. Wegst, H. Bao, E. Saiz, A.P. Tomsia, R.O. Ritchie, Nat. Mater. 14 (2015) 23–36.
[2] U.G.K. Wegst, M.F. Ashby, Philos. Mag. 84 (2004) 2167–2181.
[3] C. Wang, Y. Huang, Q. Zan, H. Guo, S. Cai, Mater. Sci. Eng. C 11 (2009) 9–12.
[4] M.A. Meyers, A.Y. Lin, P. Chen, J. Muyco, J. Mech. Behav. Biomed. Mater. 1 (2008) 76–85.
[5] A.Y. Lin, M.A. Meyers, J. Mech. Behav. Biomed. Mater. 2 (2009) 607–612.
[6] A.G. Evans, Z. Suo, R.Z. Wang, I.A. Aksay, M.Y. He, J.W. Hutchinson, J. Mater. Res. 16 (2001) 2475–2484.
[7] A.P. Jackson, J.F.V. Vincent, R.M. Turner, Proc. R. Soc. Lond. B 234 (1988) 415–440.
[8] F. Barthelat, H. Tang, P.D. Zavattieri, C.M. Li, H.D. Espinosa, J. Mech. Phys. Solids 55 (2007) 306–337.
[9] Y. Shao, H. Zhao, X. Feng, J. R. Soc. Interface 11 (2014), 20131016. .
[10] Z.Q. Liu, M.A. Meyers, Z. Zhang, R.O. Ritchie, Prog. Mater. Sci. 88 (2017) 467–498.
[11] M.R. Begley, N.R. Philips, B.G. Compton, D.V. Wilbrink, R.O. Ritchie, M. Utz, J. Mech. Phys. Solids 60 (2012) 1545–1560.
[12] F. Barthelat, J. Mech. Phys. Solids 73 (2014) 22–37.
[13] Y. Shao, H.P. Zhao, X.Q. Feng, H. Gao, J. Mech. Phys. Solids 60 (2012) 1400–1419.
[14] N. Sakhavand, R. Shahsavari, Nat. Commun. 6 (2015) 6523–6534.
[15] B. Ji, H. Gao, Mater. Sci. Eng. A 366 (2004) 96–103.
[16] S. Deville, E. Saiz, R.K. Nalla, A.P. Tomsia, Science 311 (2006) 515–518.
[17] E. Munch, M.E. Launey, D.H. Alsem, E. Saiz, A.P. Tomsia, R.O. Ritchie, Science 322 (2008) 1516–1520.
[18] M.E. Launey, E. Munch, D.H. Alsem, H.B. Barth, E. Saiz, A.P. Tomsia, R.O. Ritchie, Acta Mater. 57 (2009) 2919–2932.
[19] M.E. Launey, E. Munch, D.H. Alsem, E. Saiz, A.P. Tomsia, R.O. Ritchie, J. R. Soc. Interface 7 (2010) 741–753.
[20] V. Naglieri, B. Gludovatz, A.P. Tomsia, R.O. Ritchie, Acta Mater. 98 (2015) 141–151.
[21] H. Bai, F. Walsh, B. Gludovatz, B. Delattre, C. Huang, Y. Chen, A.P. Tomsia, R.O. Ritchie, Adv. Mater. 28 (2016) 50–56.
[22] H. Zhao, Y. Yue, L. Guo, J. Wu, Y. Zhang, X. Li, S. Mao, X. Han, Adv. Mater. 28 (2016) 5099–5105.
[23] R.F. Guo, N. Guo, P. Shen, L.K. Yang, Q.C. Jiang, Mater. Sci. Eng. A 718 (2018) 326–334.
[24] W. Cui, M. Li, J. Liu, B. Wang, C. Zhang, L. Jiang, Q. Cheng, ACS Nano 8 (2014) 9511–9517.
[25] H.L. Gao, S.M. Chen, L.B. Mao, Z.Q. Song, H.B. Yao, H. Colfen, X.S. Luo, F. Zhang, Z. Pan, Y.F. Meng, Y. Ni, S.H. Yu, Nat. Commun. 8 (2017) 287–294.
[26] H. Zhao, Y. Yue, Y. Zhang, L. Li, L. Guo, Adv. Mater. 28 (2016) 2037–2042.
[27] L.J. Bonderer, A.R. Studart, L.J. Gauckler, Science 319 (2008) 1069–1073.
[28] F. Bouville, E. Maire, S. Meille, B. Van de Moortèle, A.J. Stevenson, S. Deville, Nat. Mater. 13 (2014) 508–514.
[29] H. Le Ferrand, F. Bouville, T.P. Niebel, A.R. Studart, Nat. Mater. 14 (2015) 1172–1179.
[30] R.P. Wilkerson, B. Gludovatz, J. Watts, A.P. Tomsia, G.E. Hilmas, R.O. Ritchie, Adv. Mater. 28 (2016) 10061–10067.
[31] R.P. Wilkerson, B. Gludovatz, J. Watts, A.P. Tomsia, G.E. Hilmas, R.O. Ritchie, Acta Mater. 148 (2018) 147–155.
[32] R.O. Ritchie, Nat. Mater. 10 (2011) 817–822.
[33] R.G. Munro, J. Am. Ceram. Soc. 8 (1997) 1919–1928.
[34] W.D. Jenkins, T.G. Digges, J. Res. Natl. Bur. Stand. 48 (1952) 313–321.
[35] ASTM Standard C1211, Flexural Strength of Advanced Ceramics at Elevated Temperatures, ASTM International, West Conshohocken, PA, 2003https://doi.org/10.1520/C1211-18www.astm.org.
[36] ASTM Standard E1820, Measurement of Fracture Toughness, ASTM International, West Conshohocken, PA, 2003https://doi.org/10.1520/E1820-16www.astm.org.
[37] ASTM Standard C1259, Dynamic Young's Modulus, Shear Modulus, and Poisson's Ratio for Advanced Ceramics by Impulse Excitation of Vibration, ASTM International, West Conshohocken, PA, 2003https://doi.org/10.1520/C1259-15www.astm.org.
[38] D. Liu, B. Gludovatz, H.S. Barnard, M. Kuball, R.O. Ritchie, Nat. Commun. 8 (2017) 15942.
[39] M.G. Mueller, V. Pejchal, G. Žagar, A. Singh, M. Cantoni, A. Mortensen, Acta Mater. 86 (2015) 385–395.
[40] J.J. Kruzic, R.M. Cannon, R.O. Ritchie, J. Am. Ceram. Soc. 88 (2005) 2236–2245.